Evolution of HTO and $^{36}Cl^-$ diffusion through a reacting cement-clay interface (OPC paste-Na montmorillonite) over a time of six years

Pietro Luraschi[a,b,*], Thomas Gimmi[a,b], Luc R. Van Loon[a], Amir Shafizadeh[a,b], Sergey V. Churakov[a,b]
[a] Laboratory for Waste Management, Nuclear Energy and Safety, Paul Scherrer Institute, 5232 Villigen, Switzerland
[b] Institute of Geological Sciences, University of Bern, 3012 Bern, Switzerland

* Corresponding author
E-mail address: pietro.luraschi@psi.ch (P. Luraschi)
Keywords: cement clay diffusion porosity precipitation

Abstract

Cement and clays are proposed as sealing materials in underground repositories for radioactive waste. When cement and clay come into contact, chemical gradients between their very different porewater compositions lead to diffusive exchange of solutes, which can result in mineral transformations and alterations of transport properties at the material's interface. Small samples of cement-clay interfaces were prepared and let react over a period of six years. During this time, the changes in transport properties of the samples were periodically monitored by means of through-diffusion experiments. This technique allows studying the evolution of the diffusive flux across the reacting interface and characterizing the variation of the corresponding effective diffusion coefficient (D_e) over time. All experiments were performed on samples consisting of a hardened high porosity OPC paste and Na-montmorillonite. These model materials were chosen in order to simplify the mineralogy of the system. The experiments allowed obtaining relevant information regarding the development of the diffusive properties and the reactivity of such a cement-clay interface system. HTO and $^{36}Cl^-$ were used as tracers to study the evolution of both the total and the anion accessible porosity. After six years of reaction a considerable reduction of the flux for both HTO and $^{36}Cl^-$ was observed. The flux of HTO did, however, not approach zero, which means that connected porosity for diffusive transport of water is still available. The periodic monitoring of the sample evolution showed a strong reduction of the effective diffusion coefficient D_e of the samples within the first 1.5 years of the experiment and a less prominent decrease in the period between 1.5 and 6 years. The D_e of $^{36}Cl^-$ showed a stronger reduction compared to that of HTO; for some cells no chloride flux at all could be measured anymore at t > ~4 a. Using additional information on the extension of porosity changes from a neutron imaging study performed in parallel on the same samples, the diffusive properties of each component of the interface, or of a clay zone with reduced porosity could be estimated. For HTO the relation between the evolution of D_e and of the porosity in the clay part can be well described with Archie's empirical law. For chloride large uncertainties regarding the accessible porosity do not allow a precise correlation. Whether a complete porosity clogging will take place or some fraction of connected pore space will persist in the sample over reaction times >> than 6 years remains an open question.

1. Introduction

Several countries are planning to dispose radioactive wastes in an underground geological repository in clay-rich rock formations. Most concepts of Engineered Barrier Systems (EBS) in the geological repository foresee a wide use of cementitious materials as tunnel backfill or shotcrete liner (e.g., Nagra, 2002; IAEA, 2009; Nagra 2014). Accordingly, cement and clays will come into contact. Strong chemical disequilibrium between their pore waters will drive mass fluxes that can lead to dissolution and/or precipitation reactions and the formation of so called "skins": regions close to the interface with clearly altered physicochemical properties (Read et al., 2001; Cuevas et al., 2006; Dauzeres at al., 2010; Kosakowski and Berner, 2013). These newly formed skins may have a strong impact on safety relevant properties of the repository, such as solute and gas transport or re-saturation.

The extension and the type of alteration of these skins vary depending on the interfacing materials. Field experiments and natural analogues indicate that after years to decades of interaction the altered region extends over mm to cm scale (Tinseau et al., 2006; Fernandez et al., 2017; Mäder et al., 2017). Experimental investigations of such interfaces beyond decades are not available and their evolution on the repository timescale still remains uncertain. The quantitative understanding of reactive transport phenomena at these interfaces, that is, of the formation, extent and properties of the skins is therefore important for long-term model-based assessment of the repository under in situ conditions. To better understand the reactions taking place at such mineral interfaces, the study of natural analogues (Hodgkinson and Hughes, 1999; Martin et al., 2016; Tineasu et al., 2006; Smellie et al., 1998), laboratory experiments (e.g., Ramirez et al., 2002; Claret et al., 2002; Melkior et al., 2004; Karnland, 2004; Fernández et al., 2010) and a multitude of modelling approaches (Steefel and Lichtner, 1998; de Windt et al., 2004; Watson et al., 2009; Berner et al., 2013; Vielliard et al., 2014; Jenni et al., 2017) have been applied. Valuable reviews on the state of knowledge and future challenges regarding cement-clay interaction are provided by Gaucher and Blanc (2006), Savage (2011) and Savage and Cloet (2018). The review by Marty et al. (2014) demonstrates that the variability of modelling predictions for cement-clay interfaces in terms of porosity, mineralogical variation and position of the altered region is strongly dependent on the initial mineralogy/chemistry of the system as well as on several badly constrained model parameters. It is therefore clear that despite of the great body of research data available in this field considerable uncertainties still remain.

One of the still missing information are the properties of the skins forming at the interface when cement and clay come in contact. Especially the evolution of the diffusivity through such interfaces remains a nearly uninvestigated field where data are limited. Albinsson et al. (1996) performed diffusion experiments with different ions across clay-concrete interfaces and could estimate some diffusion coefficients. Melkior et al. (2004) studied the evolution of the HTO and chloride diffusion coefficient of bentonite after contact with alkaline porewater; and observed a decrease of the diffusivity with increasing interaction time. Yamaguchi et al. (2016) reported also a decrease of HTO diffusion coefficients to 70% of the initial value after 600 d in samples prepared from hardened cement paste and bentonite.

The present study embarks on a non-destructive methodology for studying the temporal evolution of the diffusive properties through a reacting interface composed of cement and clay material. A special cell was designed and filled with hardened high porosity cement paste and compacted Na-montmorillonite (Shafizadeh et al., 2019). These materials were chosen to build a fast reacting and relatively simple cement-clay model system. The idea was to be able to monitor the progress of the reactions within a reasonable time frame and to have a comparably simple initial chemical composition, which should facilitate the quantitative interpretation of the chemical and transport processes occurring at the interface. During six years the transport properties of the reacting samples were repeatedly investigated by measuring the steady state diffusive flux across the samples using HTO and $^{36}Cl^-$ radioactive tracers. The combined use of HTO and $^{36}Cl^-$ tracers allows quantification of diffusive transport of a neutral and a negatively charged species simultaneously. As anions are expected to be partly excluded from regions near the negatively charged clay surfaces, such data provide insight regarding the evolution of the total and the anion accessible pore space. Recently, the same samples were investigated by means of neutron imaging (Shafizadeh et al., 2015; 2020). There, the time evolution of water content across the interface was derived, which is a proxy for the porosity in the sample at saturated conditions. The observed data suggested that interactions between Na-montmorillonite and OPC result in i) a slightly increased porosity in the cement compartment close to the interface, likely related to dissolution of portlandite, and ii) a low porosity region formed within the first mm of the clay, likely related to precipitation of new mineral phases. The investigation of the same samples by means of through-diffusion experiments in the present

study makes it possible to correlate the changes in the transport properties with the reported porosity evolution. Accordingly, the evolution of the diffusivity can be interpreted taking into account the variation of the porosity across the interface.

Although this system represents a simplification, it is expected to behave similarly as an interface between OPC and bentonite (mainly composed of Na-montmorillonite, Carlson, 2004), which potentially represents an interface that will be present in a deep geological repository for radioactive waste (e.g., Nagra, 2014). The data gained for the Na-montmorillonite-OPC paste system are therefore important; at the same time, they build a good basis to investigate more complex systems.

2. Material and methods

2.1 The experimental cell

The cell was developed at the Paul Scherrer Institut (Shafizadeh et al., 2015; 2020) to allow simultaneous through-diffusion and neutron imaging investigations of cement-clay interfaces. A schematic view of the layout is shown in figure 1. The cement (1) and the clay (2) plugs (5 mm diameter, about 5 mm length, cf. table 1) were emplaced in a polytetrafluoroethylene (PTFE) cylindrical holder (3). This material is relatively flexible, resistant to the highly alkaline cement porewater, and transparent for neutrons. Mechanical stability and sample confinement is reinforced by the aluminum ring (4) around the PTFE cylinder. Polyether ether ketone (PEEK) screw caps on each side of the cells allow keeping the cell tight and the interface in contact (5). In- and outlet channels in the cap allow porewater circulation inside the cell (6). A small reservoir of ~30 mm^3 (7) is separated from the sample by a PEEK filter (8). The tightness of the cells is maintained by fluoroelastomer (FKM) O-rings (9). Possible leaking of solutes around the cell is considered as irrelevant because of the tight fit of the swelling Na-montmorillonite and the high porosity of the cement.

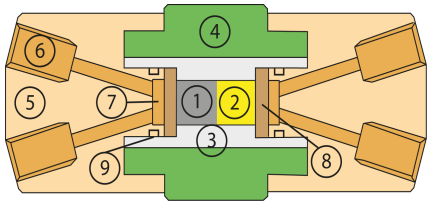

Fig. 1 Schematic view of the experimental cell used to perform through-diffusion experiments (modified after Shafizadeh et al., 2015).

2.2 Composition and preparation of samples

Na-montmorillonite and cement paste samples were prepared and saturated separately with their corresponding pore waters (table 2) and then introduced into the cell to start the interaction. Samples were kept for most of the time in a glove box under nitrogen atmosphere (24°C ± 2) to avoid potential carbonation. The cells had to be removed out of the glove box occasionally for short periods for complementary measurements. The characteristics of the interface samples are listed in table 1.

Table 1
Characteristics of the cement paste and the Na-montmorillonite in the different samples.

		Clay			Cement		
Sample	Interface contact	Length (mm)	Dry density (kg/m^3)	Porosity[1] (-)	Length (mm)	Dry density (kg/m^3)	Porosity[2] (-)
C1	14.03.2013	5.5	1670	0.40	4.5	700	0.63
C3	25.09.2013	5.0	1500	0.46	5.0	700	0.63
C4	25.06.2013	5.5	1310	0.53	4.5	700	0.63
C5	25.09.2013	5.1	1440	0.49	4.9	700	0.63
C8	02.06.2014	4.7	1540	0.45	5.3	700	0.63
C11	13.06.2014	5.0	1490	0.47	5.0	700	0.63
C15	13.06.2014	5.0	1450	0.48	5.0	700	0.63
C20	18.07.2014	4.9	1520	0.46	5.1	700	0.63
D6	25.09.2017	5.0	1560	0.44	5.0	700	0.63
D11	06.10.2017	5.0	1530	0.45	5.0	700	0.63

[1] Calculated from the dry density using a grain density of 2800 kg m^{-3}
[2] Determined by MIP (Sarott et al., 1992)

2.2.1 Na-montmorillonite

Na-montmorillonite from Milos (Greece) was converted into a homoionic form by cation exchange with a NaCl solution according to Glaus et al. (2010). The montmorillonite composition determined by XRF is listed in Shafizadeh et al. (2015). The samples were compacted to a bulk-dry density between 1310-1670 kg m^{-3} and then inserted into the cell. The compaction was performed using a dedicated press designed for this type of cell. The finally obtained bulk dry densities in the sample led to a porosity range of 0.40 – 0.53 (table 1), with the porosity values calculated according to

$$\varepsilon = 1 - \frac{\rho_b}{\rho_s}, \qquad (1)$$

where ε is the porosity (-), ρ_b the bulk dry density (kg m^{-3}) and ρ_s the grain density (kg m^{-3}). For the grain density a value of 2800 kg m^{-3} was used; similar values were considered by Muurinen (1994), Bourg et al. (2006) and Van Loon et al. (2007). Subsequently, the Na-montmorillonite plugs were saturated for 2 weeks with the corresponding porewater solution (table 2) calculated with GEMS (Kulik, 2013) according to Shafizadeh et al. (2019), with a cylindric metallic dummy occupying the space in the teflon holder foreseen for the hardened cement paste.

The interaction of the highly alkaline cement porewater with Na-montmorillonite is likely to modify the interlayer cation inside the montmorillonite. Therefore additional samples of homoionic Ca- and K-montmorillonite were prepared to measure reference diffusive properties these forms. Ca- and K-montmorillonite were produced by contacting the Na-montmorillonite with $CaCl_2$ and KCl solutions, respectively. Through-diffusion experiments were performed using the same solutions; their concentrations are given in table 6.

Table 2
Composition of the used synthetic porewater (total concentrations) for OPC (Wieland et al., 1998) and for Na-montmorillonite (Shafizadeh et al., 2019)

	OPC [M]	**Na-montmorillonite** [M]
Na	0.114	0.3
K	0.18	-
Ca	1.6×10^{-3}	-
Cl	-	0.3
S^{VI}	3×10^{-3}	-
Al	5×10^{-5}	-
pH	13.3	8.7

2.2.2 OPC cement paste

Hardened Portland cement paste (Type CEM I 52.5 N HTS, Lafarge, France) was cast about 16 years ago (Tits et al., 2003). The cement paste was produced using a special procedure (Döhring et al., 1994) and a high water cement ratio of 1.3 leading to a porosity of 63% ± 5% determined by MIP (Sarott et al., 1992). The high porosity of the cement was selected to increase the diffusivity and thus to accelerate the reactions at the interface. The cement was produced using plexiglas moulds and let hydrate at air conditions for 6 months. After that, the samples were introduced in a solution (table 2) in equilibrium with the cement (Tits et al., 2003). The samples were kept saturated all the time in the corresponding cement solution in a sealed container. A slice of about 1 cm was cut from the samples, then cylindrical samples of 5 mm diameter were drilled out of the slices. These cylinders were then placed into the cells in close contact to the Na-montmorillonite. Jakob et al. (1999) investigated the evolution of the hydraulic conductivity for the same type of cement and observed that after 3 months the hydraulic conductivity of this cement reached a constant value. Measurements performed months to years after the production indicated the same value. We assume therefore that the cement properties were not significantly changing in the following years.

The chemistry of the cement and of the cement porewater composition, which was used in the reservoirs attached to the sample, are listed in tables 3 and 2, respectively.

2.3 Through-diffusion experiments

After emplacement in the cell, the cement-clay samples were saturated for two weeks by connecting each part of the cell with a reservoir containing the corresponding porewater solution (table 2). To start the diffusion experiment the tracer had to be added to

one of the reservoirs ('high concentration side'). The tracer was inserted on the cement side in a 50 ml reservoir. For the different experiments the used activity concentration varied between 500 and 2000 Bq mL^{-1} for HTO (GE Healthcare, UK) and 500-40000 Bq mL^{-1} for $36Cl^-$ (Eckert and Ziegler, D). The reservoir connected to the clay ('low concentration side') had a volume of 20 ml and was frequently replaced to keep its concentration near zero.

The accumulated HTO and $^{36}Cl^-$ activity was subsequently measured by liquid scintillation counting (Tri-carb 2250 CA, Canberra-Packard) using Ultima Gold XR (Canberra-Packard) as scintillation cocktail, with a ratio of 5 cm^3 of sample to 15 cm^3 of cocktail. The radioisotopes were obtained from Isotope Products Europe (Blaseg, Germany). For solution preparation the reagents used were provided by Fluka (Buchs, Switzerland) or Merck (Dietikon, Switzerland), and the de-ionized ultrapure water was Milli-Q® (Merck, Switzerland).

Tritiated water is an uncharged species and should be able, in principle, to diffuse through the entire porosity domain. HTO is in general considered as a non-sorbing tracer, although Tits et al. (2003) reported some sorption on the same cement used in this experiment. A slight retardation in some cases was observed as well in the experiments discussed in this article.

Chloride-36 is negatively charged. Some aspects need to be considered while performing diffusion experiments on cement-clay interfaces with this tracer: i) due to the negative charge of the clay surfaces, $^{36}Cl^-$ diffusivity through clay samples is known to be lower than that of HTO; this feature is related to the relatively small portion of total porosity accessible for anions in montmorillonite (Pusch, 2001; Van Loon et al., 2007). ii) Glaus et al. (2010) showed how the diffusivity of $^{36}Cl^-$ in clay depends on the chloride content in the electrolyte solution. iii) On the cement side, the OPC paste contains AFm and C-S-H phases (both represent hydration products of Portland cement), on which chloride can be sorbed. Afm are a family of hydrated Ca-Al phases, which possess positively charged surfaces (Taylor, 1997). C-S-H are the main hydration product of OPC and are mainly responsible for the cement strength; they can also take up anions (Beaudoin et al. 1990; Plusquellec and Nonat, 2016). Accordingly, chloride interacts with cement when diffusing through it; such sorption phenomena have been extensively investigated in the literature (Page et al., 1981; Jensen et al., 1990; Hirao et al., 2004). During our experiments chloride sorption was observed as retardation during the transient phase; for the calculation of D_e, however, only the steady state diffusion was considered (see chapt. 2.4), which is independent of sorption.

2.4 Through-diffusion experiments: data analysis

Given the experimental set-up, diffusion can be considered as a one-dimensional process, where the tracer diffuses through a 1D domain with a length L, with a flux J. For a steady state condition, Fick's first law can be applied:

$$J = -D_e \frac{\partial C}{\partial x} \qquad (2)$$

J is the flux [Bq m^{-2} s^{-1} or mol m^{-2} s^{-1}], D_e is the effective diffusion coefficient of the sample [m^2 s^{-1}], C is the tracer concentration [Bq m^{-3}] or [mol m^3] and x is the length [m]

In a non-steady state system Fick's second law applies:

$$\frac{\partial C}{\partial t} = \frac{D_e}{\alpha} \frac{\partial^2 C}{\partial x^2} \quad , \qquad (3)$$

where t is time, α is the rock capacity, defined as:

$$\alpha = \varepsilon + \rho_b \, K_d \quad , \qquad (5)$$

K_d is the equilibrium distribution coefficient [m^3 kg^{-1}], ε the (accessible) porosity and ρ_b the bulk dry density [kg m^{-3}]. For a non-sorbing tracer K_d is zero and therefore the rock capacity is equal to the (accessible) porosity.

Eq. (3) only applies for spatially constant parameters. More generally for our cement-clay system where D_e is varying along the sample, eq. (3) has to be rewritten as

$$\alpha(x) \frac{\partial C}{\partial t} = \frac{\partial}{x} D_e(x) \frac{\partial C}{\partial x} \quad , \qquad (6)$$

Because D_e is calculated in our experiments from the steady state, $\frac{\partial C}{\partial t} = 0$ and eq. (2) can be used for the determination of the domain averaged D_e of the sample.

The effective diffusion coefficient D_e gives an indication of the diffusive properties of the sample, and can be expressed as

$$D_e = \varepsilon \frac{D_w}{G} \quad (7)$$

D_w [$m^2 s^{-1}$] is the diffusion coefficient of the species in pure water, and G [-] is a term accounting for geometrical factors (Gonzalez Sanchez et al., 2008) including the tortuosity and the constrictivity of the porous network. These two parameters are difficult to be measured separately and therefore lumped into G.

The initial and the boundary conditions are:

$$\begin{aligned} &c(x,t) = 0 && x>0 && t=0 \\ &c(0,t) = C_0 = \text{constant} && x=0 && t>0 \\ &c(L,t) = 0 && x=L && t>0 \end{aligned} \quad (8)$$

The concentration C_0 [mol m^{-3}] of the tracer on the cement side (high concentration side) is assumed to be constant, whereas $c(L,t)$ [mol m^{-3}], the concentration on the clay side (low concentration side), is assumed to be zero (Van Loon and Soler, 2003).

The flux at the low concentration side is therefore given by:

$$J(L,t) = D_e \cdot \frac{\partial c}{\partial x}|_{x=L} \quad (9)$$

Solving eq. (3) for the given initial and boundary conditions results in an analytical expression for the cumulated diffused activity A^t_{dif} [Bq] or [mol] of a tracer in the low concentration reservoir as a function of time (Crank, 1979):

$$A^t_{dif} = S \cdot L \cdot C_0 \cdot \left(\frac{D_e \cdot t}{L^2} - \frac{\alpha}{6} - \frac{2 \cdot \alpha}{\pi^2} \sum_{n=1}^{\infty} \frac{(-1)^n}{n^2} \cdot exp\left(- \frac{D_e \cdot n^2 \cdot \pi^2 \cdot t}{L^2 \cdot \alpha} \right) \right) \quad (10)$$

where S is the cross-sectional area [m^2] and t is the time [s]. At steady state conditions ($t \rightarrow \infty$) the solution reduces to:

$$A^t_{dif} = S \cdot L \cdot C_0 \cdot \left(\frac{D_e \cdot t}{L^2} - \frac{\alpha}{6} \right) \quad (11)$$

and the accumulated activity becomes a linear function of time

$$A^t_{dif} = a \cdot t + b \quad (12)$$

where

$$a = \frac{S \cdot C_0 \cdot D_e}{L} \text{ and } b = -\frac{S \cdot L \cdot C_0 \cdot \alpha}{6}$$

Thus, an average sample D_e can be derived from the slope of the accumulated activity in the linear regime (Van Loon and Soler, 2003). In such a simplified description, the resulting rock capacity α represents a combined contribution of the two components (cement and clay). The resulting value of α is therefore difficult to interpret.

2.5 Determination of the effective diffusion coefficient for the clay ($D_{e,\,clay}$) and for the clay skin ($D_{e,\,skin}$)

The measured effective diffusion coefficient represents the diffusive flux through the entire cell domain which consists of filters, clay and cement (Fig. 2). The filters need therefore to be considered in the calculation to obtain only the diffusive properties of the cement and of the clay. The filters are taken into account by considering the system as a series of resistances (Glaus et al., 2015):

$$\frac{1}{R_{tot}} = \frac{1}{R_{clay}} + \frac{1}{R_{cem}} + \frac{2}{R_{filters}} \quad (13)$$

where R is

$$R = \frac{\Delta x}{D_e} \qquad (14)$$

and Δx is the dimension of each component of the domain. Using eq. (13) the properties of the clay domain and subsequently of the clay skin can be estimated assuming known properties of all other components. We generally assumed in our analysis a constant D_e of the cement, but considered the effect of a potential alteration in the error estimation in the following section. The filter properties and the cement and clay diffusion coefficients used for this derivation are listed in table 4. Figure 3 illustrates how the diffusion coefficients of different components were determined.

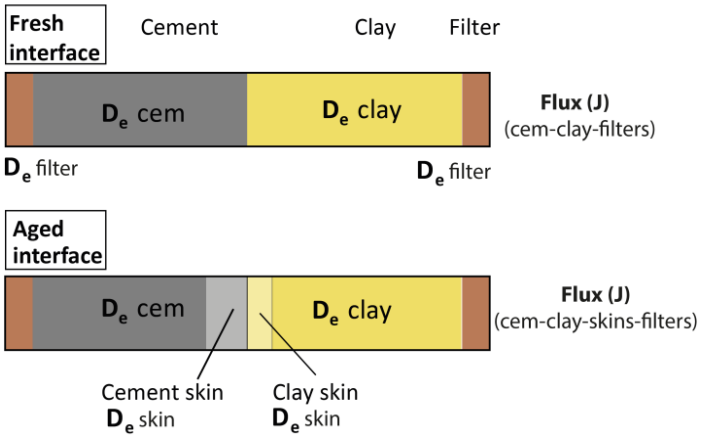

Fig. 2 Schematic view of a fresh and an aged cement-clay interface sample.

Table 3 Effective diffusion coefficients (D_e) used for calculation of the interface properties

	D_e HTO	D_e $^{36}Cl^-$	Comment
Hardened OPC paste	2.8 x 10^{-10}	1.6 x 10^{-10}	Tits et al. (2003) and Sarott et al. (1992)
Filter (Peek)	1.1 x 10^{-10}	1.1 x 10^{-10}	Glaus et al. (2008)
Na-mont. 1.5 g/cm^3	6.1 x 10^{-11}	5.2 x 10^{-12}	Present study, average value (table 6)
K or Ca-mont. 1.5 g/cm^3	1.0 x 10^{-10}	1.5 x 10^{-11}	Present study, average value (table 6)

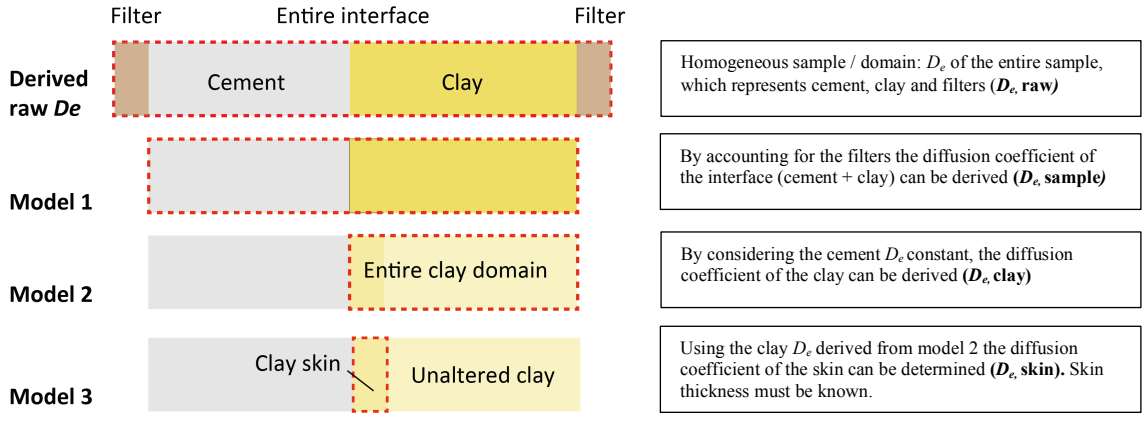

Fig. 3 Schematic representation of the region or component for which D_e was obtained. The red dashed line represents the region taken into consideration for D_e derivation in each model.

2.6 Error estimation on the derived diffusion coefficients

The estimation of the error on the total diffusion coefficient (raw D_e) was performed according to Van Loon and Soler (2003). In general, the derived diffusion coefficients have a relatively small error (~ ±6%). The errors of D_e for the other models were calculated following first order error propagation. Some additional errors may arise from (unknown) changes in filter and cement

properties, or from the choice of the steady state interval from which D_e was calculated. Glaus et al. (2008) performed diffusion experiments on similar filters as those used for the present study, and reported for filters previously used with Na-montmorillonite a decrease of up to 45% of the derived filter D_e (reaching a value of 1.1 x 10^{-10} m^2 s^{-1}). In this study for some samples the filters were exchanged during the diffusion experiments (once steady state conditions were reached since several days) to study the variation of the total diffusive properties. For the tested samples only slight variations of the flux were observed confirming the low impact of the filters on the derived sample D_e. For the $D_{e,\ sample}$ derivation we considered for both filters the value of an used filter (1.1 x 10^{-10} m^2 s^{-1}). Cement may affect less strongly the filter properties than clay, but a slight decrease of the diffusive properties is also likely to take place. Therefore, we considered the same value also for the filter on the cement side, leading to a maximum value for the derived sample diffusion coefficient ($D_{e,\ sample}$)

According to eqs. (13, 14), to derive the $D_{e,\ clay}$, the cement diffusion coefficient must be known. For our calculation $D_{e,\ cem}$ was considered similar to the one measured by Tits et al. (2003), which is 2.8 x 10^{-10} m^2 s^{-1} (cement porosity: 0.63). This assumption is based on observations made by Sarott et al. (1992) on cement samples produced in the same way, where hydraulic conductivity was measured over longer period, concluding that the hydration was largely completed after 3 months and that the hydraulic conductivity remains constant after that time. Moreover the samples were stored under nitrogen atmosphere, strongly reducing the carbonation chances, which may influence the cement diffusive properties. Although the cement properties are not expected to be significantly altered, we estimated the effect of a modified cement diffusion coefficient ($D_{e,\ cem}$) on the derived $D_{e,\ clay}$ (Fig. 4a). We furthermore estimated the error arising from neglecting the alteration of the diffusion properties of the cement skin. Shafizadeh et al. (2019) observed on the cement side porosity variations with a local maximum of +10% porosity. The impact of this cement skin (with different spatial extension) is shown in Figure 4b.

The high porosity of the used cement paste results in a high $D_{e,\ cem}$. Therefore, according to eq. (13), a variation of the cement diffusion coefficient would only slightly affect the derived $D_{e,\ clay}$. Furthermore, with increasing interaction time the formation of the low-porosity region inside the clay further reduces the overall diffusivity of the system, making the variation of the cement properties progressively less influent. Thus, a modification of the cement diffusion coefficient, or the formation of a cement skin with slightly altered porosity will have little impact on the derived clay diffusion coefficient as clearly visible in Figures 4a and 4b.

For the error estimation we considered a variation of the filters and the cement properties of 10% (on the initial value). This led to a general error of ~ ± 20% for the entire clay domain (model 2). For the skin region (model 3), additional uncertainties (e.g., skin extension, unaltered clay D_e) increased the propagated error up to ± 45%.

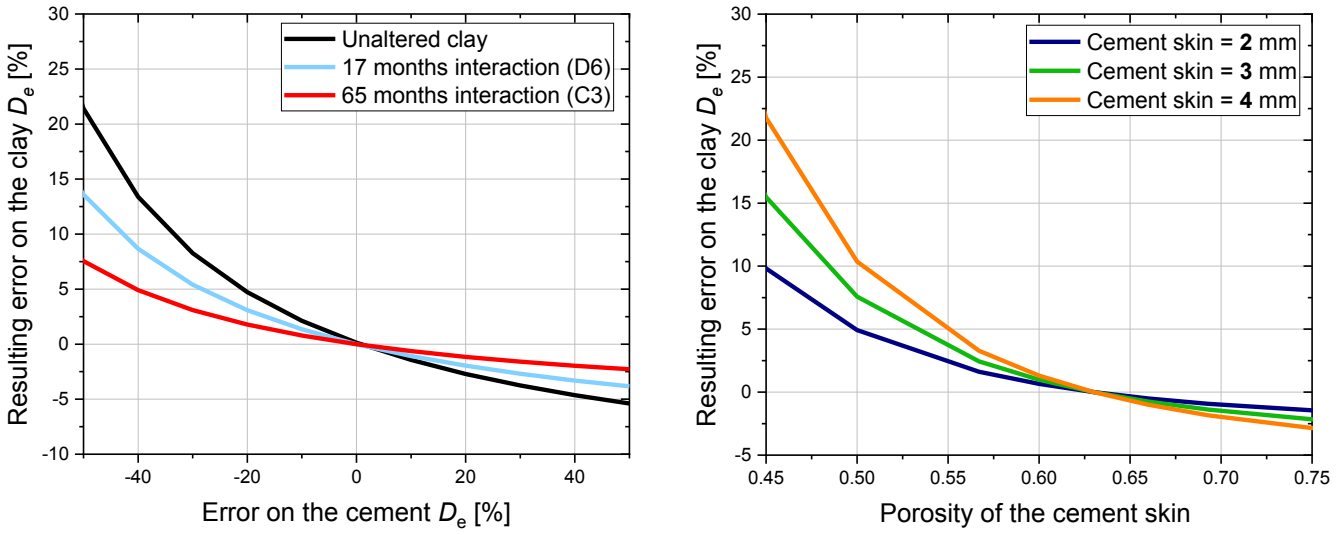

Fig. 4 Variation of the derived diffusion coefficient D_e of the clay part (in %) upon a variation of the diffusion properties of the cement part. (a) Variation of D_e clay depending on the hypothetical error of the used D_e of the cement part. The three lines represent different interaction times of the cement-clay interface. (b) Variation of D_e clay depending on assumed porosity and extent of cement skin, at an interaction time of 65 months. The longer the interaction time, the smaller is the influence of the cement skin properties on D_e of the clay part.

3. Results

3.1 HTO through-diffusion experiments

The data shown in Fig. 5a, representing the derived raw D_e (filters, cement and clay), can be divided into two subgroups. For the first subgroup (red symbols in Fig. 5a), a remarkable reduction of the determined D_e during the first 12 to 17 months is observed, followed by a subsequent moderate reduction until 73 months. There is a certain scatter between the data obtained on different cement-clay samples for this subgroup. This fact is certainly related to i) slight variations in the density of the clays and ii) slight variations in the length of the cement and clay parts of the samples (see table 1), possibly also to iii) partial clogging of filter pores, leading to a decrease of the diffusive properties of the entire system, or also iv) small fractures or heterogeneities which may occur during the insertion or during the reaction of the cement with the clay, resulting in diffusivity change. The second subgroup showed a clearly different overall trend: the D_e of these samples does not significantly vary over time (blue squares, Fig. 5a), it decreases only slightly with respect to the initially measured values. Shafizadeh et al. (2019) using neutron imaging did not detect any significant porosity variation for such samples; the reason why the low porosity region did not form in these samples is unclear and under investigation. Table 4 resumes the derived effective diffusion coefficients for all the interface samples that were measured.

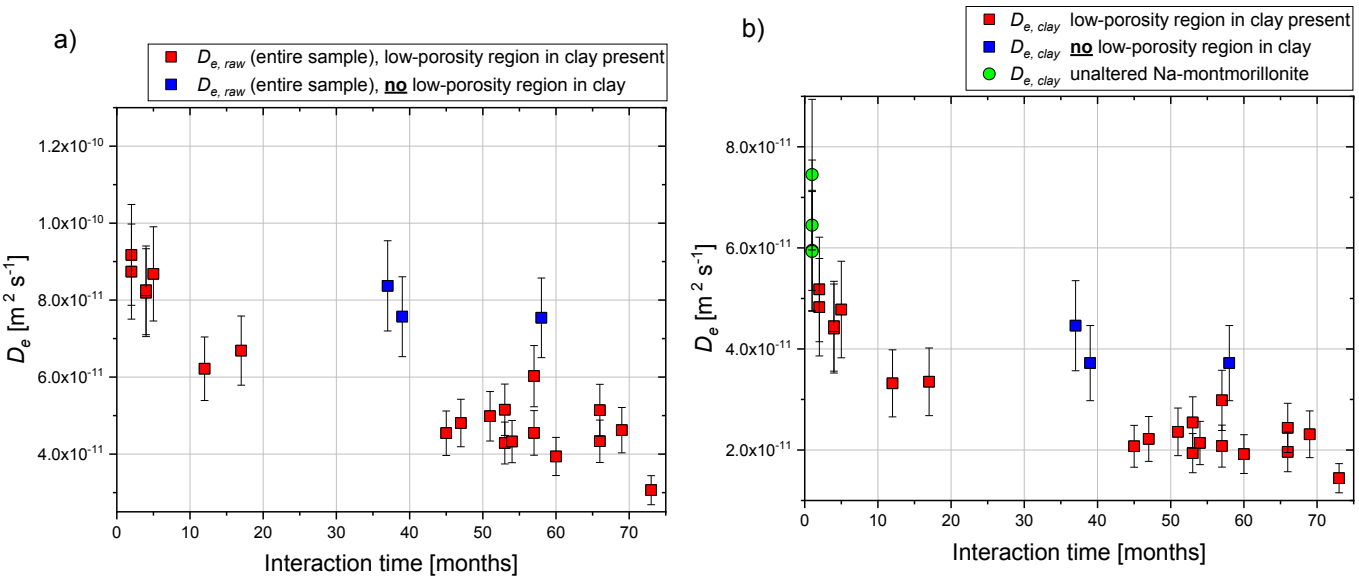

Fig. 5 Evolution of the average diffusion coefficient (D_e) of HTO for **a)** the entire system ($D_{e, raw}$) composed of filters, cement and clay); and **b)** for the clay part only ($D_{e, clay}$).

From the raw D_e values (Fig. 5a), first the D_e values of the entire samples ($D_{e, sample}$) consisting of cement and clay were calculated according to Eq. (13) and Table 1. In order to reduce the variability in the derived diffusion data caused by the slight variation of the clay and cement domain sizes, effective diffusion coefficients for the clay part ($D_{e, clay}$) were then calculated from the overall sample diffusion coefficients ($D_{e, sample}$), assuming that the main changes affecting diffusion occurred in the clay. This assumption is based on the results of Shafizadeh et al. (2020), who reported a region with only slightly higher porosity developing on the cement side of the interface, but a low porosity region of about 1 mm developing on the clay side close to the interface. The derived average D_e of the ~5 mm clay plug represents the properties of the region with unvaried porosity (unaltered clay), and the properties of the skin (Fig. 3). Assuming a constant effective diffusion coefficient in the cement plug equal to the one reported by Tits et al. (2003), D_e values for the clay part were obtained using eq. (13) (Fig. 5b). The general trend is similar to the one observed for the derived $D_{e, raw}$ (Fig. 5a): a strong decrease of diffusivity during the first 12 to 17 months and a subsequent slower D_e decrease after 17 months. The scatter between the data points became visibly smaller compared to that of the raw D_e shown in Fig. 5a, confirming that an important variability of the sample D_e is related to the variability of the lengths of the cement and clay part. The remaining variabilities are probably related to minor variations of the material density (and composition) and the contamination of filters.

The earliest measured D_e value for the clay region, defined as the average value after 2-4 months, is 4.7 x 10^{-11} m^2 s^{-1}, which is lower than values measured for unaltered Na-montmorillonite samples at a similar density (green circles Fig. 5b; table 6). One has to keep in mind that any variation of the cement or of the filters diffusion coefficient directly affects the derived D_e value of the clay. But more importantly, this 'initial' D_e of the clay region represents a value after 2-4 months of interaction, due to the time needed to perform the through-diffusion experiments. The difference between this 'initial' value and that of unaltered Na-montmorillonite means that reactions at the interface already occurred and possibly a skin already started forming, leading to a decrease of the D_e. After 12 to 17 months the $D_{e,\,HTO}$ rapidly decreased to 3.3 x 10^{-11} m^2 s^{-1}. Between 17 and 73 months the $D_{e,\,HTO}$ decreased further to an average value of 2.2 x 10^{-11} m^2 s^{-1}. Interestingly from 45 to 73 months the $D_{e,\,HTO}$ remained quite stable. This fact suggests that from 45 months the interface reactivity is clearly reduced. Since no data were obtained between 17 and 45 months of interaction it is possible that the reactivity of the interface was reduced already earlier.

Table 4
Effective diffusion coefficients of HTO for the various regions of the clay domain (subdivided in 4 parts, see Fig. 4). Raw D_e: obtained D_e for sample and filters. Model 1: the interface sample (cement, clay). Model 2: the entire clay region. Model 3: skin region evaluated assuming either a diffusion coefficient of Na-montmorillonite (model 3a) or of K, Ca-montmorillonite (model 3b) for the for unaltered clay part (table 4). For the $D_{e,\,skin}$ calculation, a skin thickness of 1mm was used (2 mm for C1) according to Shafizadeh et al. (2019, 2020).

Sample	interaction time (months)	D_e of the entire sample (D_e raw)	D_e interface without filters (Model 1)	D_e of the entire clay domain, (Model 2)	D_e of the skin region. Unaltered clay = Na-mont. (Model 3a)	D_e of the skin region. Unaltered clay = Ca, K-mont. (Model 3b)
C1	12	6.2 x 10^{-11}	5.5 x 10^{-11}	3.3 x 10^{-11}	2.1 x 10^{-11}	1.5 x 10^{-11}
	54	4.3 x 10^{-11}	3.7 x 10^{-11}	2.1 x 10^{-11}	1.1 x 10^{-11}	9.0 x 10^{-12}
	60	3.9 x 10^{-11}	3.3 x 10^{-11}	1.9 x 10^{-11}	9.2 x 10^{-12}	7.9 x 10^{-12}
	73	3.1 x 10^{-11}	2.5 x 10^{-11}	1.4 x 10^{-11}	6.4 x 10^{-12}	5.8 x 10^{-12}
C3	5	8.7 x 10^{-11}	8.2 x 10^{-11}	4.8 x 10^{-11}	2.6 x 10^{-11}	1.5 x 10^{-11}
	47	4.8 x 10^{-11}	4.1 x 10^{-11}	2.2 x 10^{-11}	6.3 x 10^{-12}	5.4 x 10^{-12}
	53	4.3 x 10^{-11}	3.6 x 10^{-11}	1.9 x 10^{-11}	5.2 x 10^{-12}	4.6 x 10^{-12}
	66	4.3 x 10^{-11}	3.7 x 10^{-11}	2.0 x 10^{-11}	5.3 x 10^{-12}	4.6 x 10^{-12}
D6	2	8.7 x 10^{-11}	8.2 x 10^{-11}	4.8 x 10^{-11}	2.6 x 10^{-11}	1.6 x 10^{-11}
	4	8.2 x 10^{-11}	7.6 x 10^{-11}	4.4 x 10^{-11}	2.1 x 10^{-11}	1.3 x 10^{-11}
	17	6.7 x 10^{-11}	6.0 x 10^{-11}	3.3 x 10^{-11}	1.2 x 10^{-11}	9.1 x 10^{-12}
D11	2	9.2 x 10^{-11}	8.7 x 10^{-11}	5.2 x 10^{-11}	3.2 x 10^{-11}	1.7 x 10^{-11}
	4	8.3 x 10^{-11}	7.7 x 10^{-11}	4.4 x 10^{-11}	2.1 x 10^{-11}	1.4 x 10^{-11}
C5	51	5.0 x 10^{-11}	4.3 x 10^{-11}	2.4 x 10^{-11}	6.7 x 10^{-12}	5.7 x 10^{-12}
	53	5.2 x 10^{-11}	4.4 x 10^{-11}	2.5 x 10^{-11}	7.3 x 10^{-12}	6.0 x 10^{-12}
	66	5.1 x 10^{-11}	4.5 x 10^{-11}	2.4 x 10^{-11}	7.2 x 10^{-12}	6.0 x 10^{-12}
C15	45	4.5 x 10^{-11}	3.9 x 10^{-11}	2.1 x 10^{-11}	5.7 x 10^{-12}	5.0 x 10^{-12}
	57	6.0 x 10^{-11}	5.3 x 10^{-11}	3.0 x 10^{-11}	9.6 x 10^{-12}	7.6 x 10^{-12}
C8	39	7.6 x 10^{-11}	6.9 x 10^{-11}	3.7 x 10^{-11}	-	-
	58	7.5 x 10^{-11}	6.9 x 10^{-11}	3.7 x 10^{-11}	-	-
C20	37	8.4 x 10^{-11}	7.8 x 10^{-11}	4.5 x 10^{-11}	-	-
C11	57	4.5 x 10^{-11}	3.9 x 10^{-11}	2.1 x 10^{-11}	5.7 x 10^{-12}	5.0 x 10^{-12}
C4	69	4.6 x 10^{-11}	3.9 x 10^{-11}	2.3 x 10^{-11}	6.1 x 10^{-12}	5.2 x 10^{-12}

3.2 $^{36}Cl^-$ through-diffusion experiments:

Effective $^{36}Cl^-$ diffusion coefficients derived from samples at different interaction times (Fig. 6 and table 5) show a similar trend as observed for the HTO tracer: a strong reduction of the D_e after 17 months and a more gentle reduction in the subsequent years. The relative reduction in chlorine diffusivity is, however, much stronger than the relative reduction measured with HTO. The earliest derived $D_{e,\,Cl}$ for the whole clay domain, obtained after 2 months of interaction time from one cell only, is 8.4 x 10^{-12} m^2 s^{-1}, which is slightly higher than the 5.2 x 10^{-12} m^2 s^{-1} measured for unaltered Na-montmorillonite. After 17 months the $D_{e,\,Cl}$ drastically decreased to 2.2 x 10^{-13} m^2 s^{-1}. The three measurements after more than 55 months of interaction indicate variable values between 1.5 x 10^{-14} and 2.5 x 10^{-13} m^2 s^{-1}.

The obtained $D_{e,\,Cl}$ show a relatively large scatter. This is related to the sensitivity of the tracer with respect to the media through which it diffuses: small changes in compaction, a preferential transport pathway or variation in filter properties may have a very strong influence on the calculated chloride diffusivity. Also, the reduction of D_e is so strong that the activity measurements partly approach the detection limit. For this reason repeated experiments with different initial activities were performed. It has to be noted that several samples did not show any $^{36}Cl^-$ flux even when using the highest initial activity (40 kBq/ml). Furthermore, as mentioned in the previous section, not all the samples reacted similarly: some of them show a very small reduction of the diffusive flux over time. In one of these samples (where porosity hardly evolved, as observed by Shafizadeh et al. (2015; 2020) the D_e of $^{36}Cl^-$ changed similarly as that of HTO. In fact, the $D_{e,\,Cl}$ was only slightly lower than the initial value in this sample (orange symbol, Fig. 6).

Table 5 Effective diffusion coefficients for $^{36}Cl^-$ for the various regions of the clay domain (subdivided in 4 parts, see Fig. 4). Raw D_e: obtained D_e for sample and filters. Model 1: the interface sample (cement, clay). Model 2: the entire clay region. Model 3: skin region evaluated assuming an average diffusion coefficient of Na-montmorillonite for the unaltered the clay part (table 4). For the $D_{e,\ skin}$ calculation, a skin thickness of 1mm was used according to Shafizadeh et al. (2020).

Sample	interaction time (months)	D_e of the entire sample (D_e raw)	D_e interface without filters (Model 1)	D_e of the entire clay domain, (Model 2)	D_e of the skin region. Unaltered clay = Na-mont. (Model 3)
D11	2	2.0×10^{-11}	1.6×10^{-11}	8.4×10^{-12}	-
	4	1.5×10^{-11}	1.2×10^{-11}	6.4×10^{-12}	-
D6	17	5.7×10^{-13}	4.4×10^{-13}	2.2×10^{-13}	4.6×10^{-14}
C4	69	3.1×10^{-13}	2.4×10^{-13}	1.3×10^{-13}	2.5×10^{-14}
C11	57	3.8×10^{-14}	2.9×10^{-14}	1.5×10^{-14}	3.0×10^{-15}
C15	57	6.4×10^{-13}	4.9×10^{-13}	2.5×10^{-13}	5.1×10^{-14}
C8	58	1.4×10^{-11}	1.1×10^{-11}	5.5×10^{-12}	-

4. Discussion

4.1 Interface reactivity: evolution of diffusivity and porosity

The observed changes of the diffusive fluxes for HTO and chloride indicate a strong reduction of the D_e of the entire sample ($D_{e,\ sample}$), or also of the clay part ($D_{e,\ clay}$), during the first 12 to 17 months and a subsequent slower reduction. According to eq. (7) a reduction of the diffusion coefficient is related to a decrease of the (average) porosity (ε) and an increase of the geometrical factor (G), which includes the tortuosity. The strong chemical differences between cement and clay porewater trigger mass fluxes at the material interface and lead to quick mixing of the porewater in the interface region. This change in the pore water composition induces dissolution-precipitation reactions and mineralogical changes, which affect both the porosity and the geometry of the pores.

Analysis of the samples conducted by Shafizadeh et al. (2015; 2020) showed a reduction of the porosity inside the first mm of the clay and a slight increase of porosity on the cement side. This porosity evolution certainly affects fluxes measured in our through-diffusion experiments. At the same time, the remaining part of the clay region without clear porosity evolution, which was called "unaltered or unreacted clay part", may have undergone chemical changes too. Due to the high alkalinity of the cement porewater and the higher cation exchange selectivity of montmorillonite for Ca and K compared to Na, the montmorillonite is expected to transform from the initial Na form into a K and Ca form near the interface. As cation exchange reactions are fast compared to mineral alterations, it is likely that this transformation into a K and Ca form has extended clearly beyond the zone of altered porosity, possibly throughout the whole clay plug. Ca- and K-montmorillonite have different diffusive (Gonzalez Sanchez et al., 2008) and swelling properties (Karnland, 2006) compared to Na-montmorillonite. Gonzalez Sanchez et al. (2008) investigated diffusion coefficients of Ca and Na-montmorillonites for a bulk dry density of 1900 kg m^3 and two different ionic strengths. In these experiments the D_e of HTO in Ca-montmorillonite was found to be about ~60% higher than that in Na-montmorillonite. In the experiments performed during the present study, for a compaction of 1500 ± 100 kg m^3 the D_e of HTO in Ca- and K-montmorillonite were found to have similar values, and were ~40% higher than the D_e of HTO in Na-montmorillonite. Thus the dependence of the HTO diffusivity on the composition of the montmorillonite needs to be considered while dealing with the evolution of the diffusivity of the clay at the interface. Preliminary (unpublished yet) investigation on the present samples by means of SEM/EDX, indicate a partial transformation of Na-montmorillonite into the Ca and K form, as already described in the literature (Mosser-Ruck and Cathelineau, 2004; Gaucher and Blanc, 2006).

The stronger reduction of the diffusion coefficient of chloride with respect to HTO is related to the montmorillonite structure. The distinction of different pore environments in clays (Fig. 7) and the magnitude of diffusive fluxes or generally of solute transport in these environments remain a matter of debate (Wersin et al., 2004; Appelo, 2013). Often the total porosity in clay rocks is subdivided into i) free porosity, a domain with a charge balanced electrolyte solution, ii) interlayer porosity between single TOT layers of swelling clay minerals, containing hydrated cations that compensate the negative structural charge, and iii) diffuse double layer (DDL) porosity, containing water, charge compensating cations and anions. Interlayer water is generally thought to contain mainly (or even only) cations, whereas the DDL displays an excess of cations and the free porosity is charge neutral (Mitchell and Soga, 1992; Bradbury and Baeyens, 2003; Appelo, 2013). Interlayer and diffuse double layer are partly also considered as a single compartment, which can be described by a Donnan approach (Jenni et al., 2017), where the Donnan pore water contains also an excess of cations. At a bulk dry density of 1500 kg m^3 most of the porosity of Na-montmorillonite is interlayer porosity (Pusch,

2001). Precipitation of new mineral phases is thought to occur preferably in the free porosity. Interlayer pores are expected to be less accessible or inaccessible for anions. Therefore precipitation of new minerals taking place in the free porosity is expected to affect the chloride flux more strongly than the HTO flux. This conclusion is supported by the observed evolution of the diffusion coefficients ratio: the initial $D_{e,\,HTO}/D_{e,\,Cl}$ for unaltered Na-montmorillonite samples is about 10; after 17 months of reaction this ratio is around 150. At longer interaction times, ratios between 120 and 1400 were obtained. It has to be noted that in several cells no chloride flux at all could be measured after 6 years of interaction, even though the initial activity at the inlet was increased in repeated experiments to possibly overcome the detection limit at the low concentration side for very low $^{36}Cl^-$ fluxes. For the cells where no $^{36}Cl^-$ flux was detected, it can be stated that the diffusion coefficient of the entire sample had to be lower than 10^{-14} m^2 s^{-1} (no flux observed with a C_0 activity of 40 kBq/ml), which indicates an almost complete blocking of the anion accessible porosity.

Mineralogical investigation and simulation of bentonite-OPC interaction made by other authors indicate the possible formation of many different mineral phases, depending on the system composition and condition (Cuevas et al., 2006; Savage et al., 2007; Fernandez et al., 2018). In our case the nature of the phase/s precipitating is currently under investigation; but the experimental conditions (CO_2 free environment and ambient temperature) suggest that carbonates and/or zeolite are unlikely to be the major phase responsible for the porosity decrease.

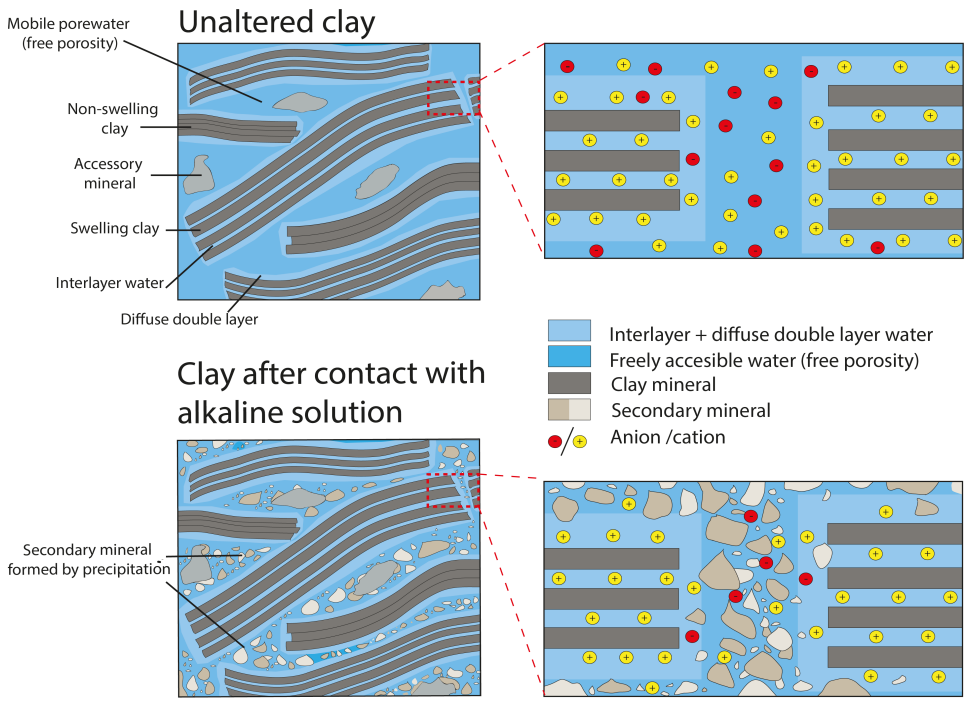

Fig.7 Schematic illustration of clay minerals and respective pore environments for unaltered clay, and for clay after contact with alkaline solution (e.g. cement porewater). Precipitation location (free porosity only or interlayer/ diffuse double layer) and precipitation type (homogeneous vs heterogeneous) are not clear.

Table 6
Summary of D_e values for HTO and Cl in various montmorillonites and Bentonites (MX-80) from literature and measured in the present work.

Author	HTO Na-mont.	$^{36}Cl^-$ Na-mont.	HTO Ca-mont.	$^{36}Cl^-$ Ca-mont.	HTO K-mont.	$^{36}Cl^-$ K-mont.	Comment	Bulk dry density
Glaus et al. (2010)	1.7×10^{-11}	7.2×10^{-14}					0.1 M NaClO4	1900 kg m^3
		2.5×10^{-13}					0.5 M NaClO4	1900 kg m^3
	1.9×10^{-11}	4.7×10^{-13}					1.0 M NaClO4	1900 kg m^3
		7.2×10^{-13}					2.0 M NaClO4	1900 kg m^3
Gonzalez et al. (2008)			3.5×10^{-11}				0.5 M CaCl2	1900 kg m^3
			3.7×10^{-11}				0.005 CaCl2	1900 kg m^3
	1.4×10^{-11}						1.0 M NaCl	1900 kg m^3
	1.5×10^{-11}						0.01 M NaCl	1900 kg m^3
Melkior et al. (2004)	7.4×10^{-11}	5.5×10^{-12}					*Bentonite sample	1700 kg m^3
	7.3×10^{-11}						*Bentonite sample	1700 kg m^3
	4.4×10^{-11}	1.5×10^{-12}					*Bentonite sample	2000 kg m^3
	4.2×10^{-11}						*Bentonite sample	2000 kg m^3
Melkior et al. (2009)	5.3×10^{-11}		5.1×10^{-11}				*Bentonite sample	1600 kg m^3
	5.0×10^{-11}		5.1×10^{-11}				*Bentonite sample	1600 kg m^3
Present Study								
P_Na1	6.0×10^{-11}	4.8×10^{-12}					0.3 M NaCl	1450 kg m^3
P_Na2	5.9×10^{-11}	5.0×10^{-12}					0.3 M NaCl	1450 kg m^3
P_Na1B	6.5×10^{-11}						0.3 M NaCl	1550 kg m^3
P_Na2B	$^{*}7.5 \times 10^{-11}$	5.7×10^{-12}					0.3 M NaCl	1520 kg m^3
P_K1					1.1×10^{-10}	2.7×10^{-11}	0.3M KCl	1450 kg m^3
P_K2					8.8×10^{-11}		0.3M KCl	1450 kg m^3
P_Ca1B			1.0×10^{-10}	1.3×10^{-11}			0.1M $CaCl_2$	1450 kg m^3
P_Ca2B			1.2×10^{-10}	4.6×10^{-12}			0.1M $CaCl_2$	1450 kg m^3

*value not considered to obtain average unaltered Na-montmorillonite D_e

4.2 Temporal development of the reactivity at the interface

The D_e evolution of the clay domain (model 2 see Fig. 4) for both HTO and $^{36}Cl^-$ (Fig. 5 and 6) give an estimate of a characteristic time required for substantial mineral transformations at the interface. Two distinct phases could be identified: a first period (0-17 months) related to a strong decrease of the diffusivity (46% $D_{e,\ HTO}$ reduction, and ~ 96% decreases for $D_{e,\ Cl}$) and a second period (17-73 months) with moderate decrease of the D_e. It was further noted that the $D_{e,\ HTO}$ remained quite stable during the period between 45 and 73 months. The two periods with different evolution of the diffusive properties are likely related to stages of dissolution-precipitation reactions occurring at the interface. Although only limited data are available at the moment, it can be hypothesized that most of the reactions occurred already during the first 1.5 year. For the same samples, Shafizadeh et al. (2020) observed by means of neutron imaging a strong porosity reduction in the clay within the first 17 months and a less prominent porosity decrease after this period. The porosity reduction following mineral reactions slows down diffusive mass transfer and thus reduces the further reactivity of the interface. This trend was observed as well in field experiments (Mäder et al., 2017) or in numerical simulation (Kosakowski and Berner, 2013)

4.3 Considerations on the skin properties

Measurements performed by Shafizadeh et al. (2020) provide an estimate of the thickness (~1mm) of the low porosity alteration zone developing inside the clay. According to eqs. (13) and (14), by making some assumption as previously discussed, it is possible to derive a rough estimation of the diffusive properties of the clay skin. The obtained values are only an approximation because of other unknown factors such as changes in the diffusive properties of filters, and the slight variation of cement porosity (Shafizadeh et al., 2020). Nevertheless, it can be assumed with high confidence that the low porosity region in the clay compartment next to the interface represents the bottleneck domain which limits the overall HTO and ion flux through the interface. In such a system slight changes in the diffusive properties of cement or of the filters should have a minor impact on the overall properties of the sample. The clay domain was split in two regions: an unaltered clay compartment and an altered skin at the interface (Fig. 8a and b). As has been discussed earlier the diffusive properties of the clay with more or less unaltered porosity are not certain. Some chemical reactions (e.g. cation exchange in the interlayer) are very likely to take place on the time scale of the experiments due to the high contents of K^+ and Ca^{2+} of the cement porewater. Therefore the calculated skin parameters are subject to relatively large uncertainties. The diffusion coefficient of montmorillonite can vary remarkably depending on its cationic composition (Table 7). Assuming that all montmorillonite turned into Ca- or K-montmorillonite via cation exchange, the calculated $D_{e,\ HTO}$ of the skin is lower by about 27%

(0 and 17 months interaction) or about 15% (>45 months interaction) compared to assuming the clay remained Na-montmorillonite (Fig. 8a). In the former case, $D_{e,\ skin}$ for HTO becomes ~1.2 x 10^{-11} after 12-17 months of interaction and reaches an average value of 6 x 10^{-12} between 45 and 73 months. In the latter case, the clay skin D_e for HTO after 12-17 months becomes ~1.7 x 10^{-11} m^2 s^{-1} and reaches an average value of 7 x 10^{-12} between 45 and 73 months.

Regarding chloride (Fig. 8b), the measured diffusivity values are so low and their variability at later times so large that considering the diffusive properties of the unreacted clay part as that of Na-montmorillonite or of K or Ca- montmorillonite does hardly affect the resulting diffusion coefficients obtained for the skin. After 17 months of interaction the chloride $D_{e,\ skin}$ is calculated as 4.6 x 10^{-14} m^2 s^{-1}; at more than 55 months the $^{36}Cl^-$ $D_{e,\ skin}$ varies between 5.1 x 10^{-14} and 3.0 x 10^{-15} m^2 s^{-1}.

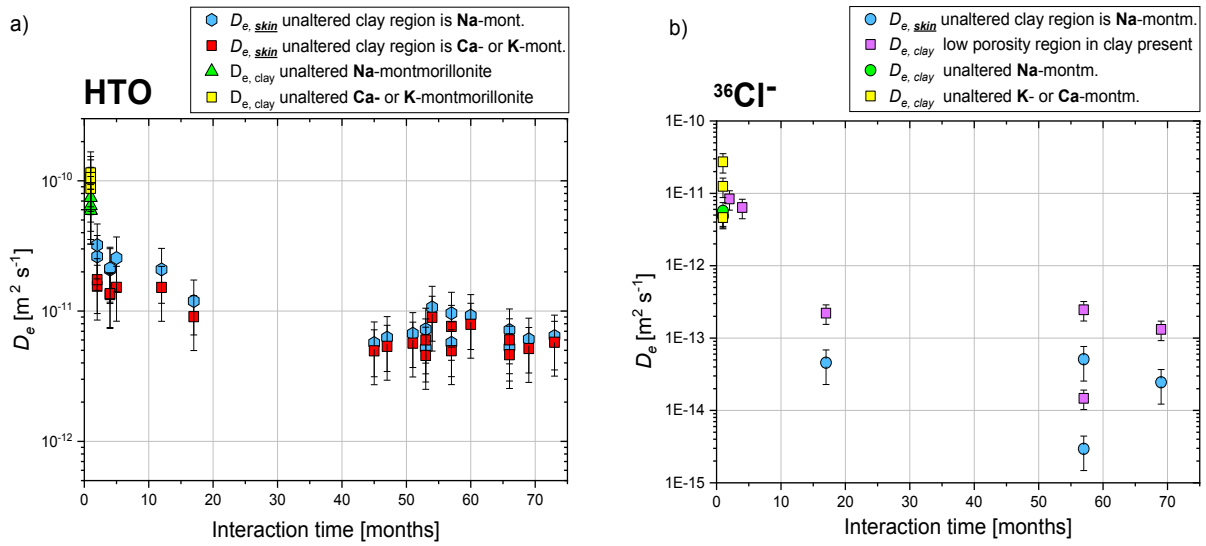

Fig. 8 a) Evolution of the effective HTO diffusion coefficient of the clay skin ($D_{e,\ skin}$). The diffusion coefficient is calculated considering the unreacted part of the clay as Na-montmorillonite (blue) or K/Ca-montmorillonite (red). **b)** Evolution of the effective diffusion coefficient, for $^{36}Cl^-$, of the entire clay domain (pink) and of the clay-skin (light blue). The diffusion coefficient of the skin ($D_{e,\ skin}$) is calculated considering the unreacted part of the clay as Na-montmorillonite.

4.4 Relation to Archie's law

The effective diffusion coefficient and the porosity can often be correlated according to a relationship given by Archie (1952),

$$D_e = D_w\, \varepsilon^m \qquad (15)$$

where m is a cementation factor [-], which depends on the connectivity and the geometry of the pores and is rock specific. Several modified versions of this relationship were used to describe different rock properties (Boudreau, 1996; Muurinen, 1994; Rosanne et al., 2003; Van Loon et al., 2014; Tyagi et al., 2013). Fig. 8 displays in a logarithmic plot the conventional Archie's relationship for some literature data and the D_e of HTO for Na-montmorillonite derived in the present study (for estimation of the $D_{e,\ skin}$ the unaltered clay part was considered to be Na-montmorillonite). For unreacted fresh samples the porosity values were calculated according to eq. (1). For the skin region in the montmorillonite the porosity was estimated based on the measurements performed by Shafizadeh et al. (2020). Porosity values for the skins have a considerable uncertainty, since the estimation of the thickness, of the porosity and the definition of the skin itself is not straightforward. The HTO data, including those of the reacted clay skins, can be approximately described by Archie's relationship using a cementation factor of m = 4.4, The other way round, this means also that Archie's relationship may be used in numerical simulations, which aim at modelling Na-montmorillonite contacting cement or alkaline porewater, to estimate the diffusive properties of such newly forming skins based on the evolving porosity.

The analogous plot for the chloride diffusion coefficients is more controversial and more difficult to interpret. This fact is related to the uncertainty of the estimation of the anion accessible porosity. For unreacted clay samples the anion accessible porosity was estimated based on data in Van Loon et al. (2007). For the skin-regions the average total porosity of ~30% estimated from the data of Shafizadeh et al. (2020) would relate to an anion accessible porosity of less than 2% according to Van Loon et al. (2007). It has to be mentioned that Van Loon et al. (2007) use porosities for differently compacted samples, whereas in our case porosities were reduced

by mineral precipitations. Precipitation is likely to take place in the free porosity, drastically reducing the anion accessible porosity (Fig. 7). Accordingly, the anion accessible porosity estimated for our skins in this way is very uncertain, leading to a large uncertainty when estimating a cementation exponent with Archie's empirical law. In fact, due to the very large uncertainty of the anion accessible porosity of the skins, it cannot be decided whether or not the skin data follow the same trend as the other data. Nevertheless the very low diffusivity values measured (in some cases no flux was observed) suggest that only a very small portion of the porosity remains available for anions.

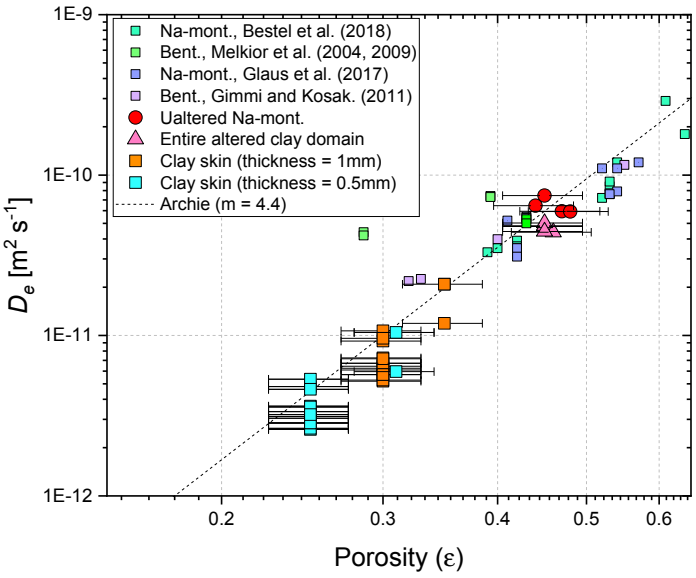

Fig. 9 Relationship between the effective HTO diffusion coefficient and the diffusion accessible porosity for Na-montmorillonite (and bentonite), with data from the literature and values reported here. The dashed line represents the classical Archie's relation, eq. (15) with m = 4.4. Porosities for the skin regions were derived from the data of Shafizadeh et al. (2020); the error on these porosities is estimated to be ±10%.

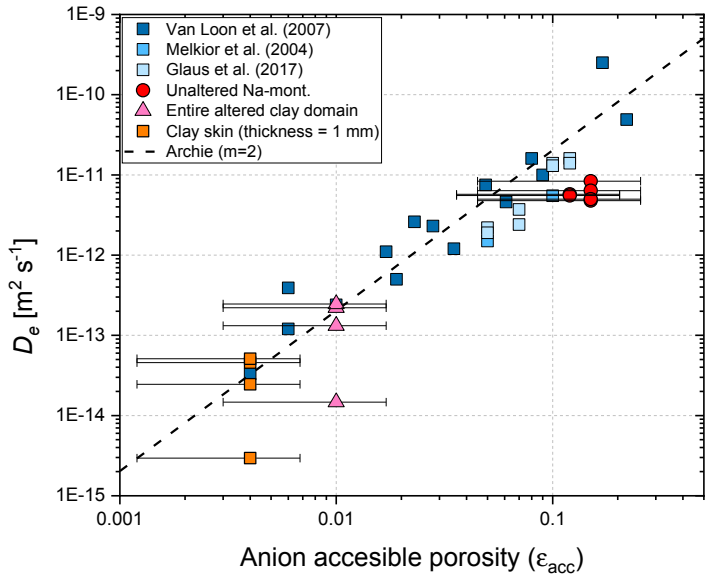

Fig. 10 Relationship between the effective $^{36}Cl^-$ diffusion coefficient and the diffusion accessible porosity for chloride in Na-montmorillonite (and bentonite), with data from the literature and derived in this study. The dashed line represents the classical Archie's relation (Eq. 15) with m = 2. Porosities for the entire clay domain (pink) and the clay skin (orange) are only rough estimates with very large uncertainties.

4.5 Transferability and implications for other cement-clay systems and other processes

The mineralogy of the interface samples studied in this work was intentionally kept as simple as possible to facilitate the interpretation of the measurement. Using cement-claystone samples or concrete-bentonite samples made of materials as will be used in disposal sites is very complex in terms of handling, sample preparation, characterisation and interpretation of the observations, mainly due to the high heterogeneity of the phases and their chemical variability. The exact parameters of mass transport, interaction kinetics and the consequent mineral reactions modifying the transport properties of interfaces are expected to depend on the specific materials. Despite the simplicity, the samples prepared from Na-montmorillonite and OPC paste studied in this work are a good proxy to a bentonite-OPC interface that is foreseen in a geological repository for radioactive wastes (e.g., Nagra, 2002). Bentonite (MX-80) contains up to 85% of Na-montmorillonite. Other minerals are quartz, feldspars, calcite and accessory minerals in minor amounts (Carlson, 2004). The accessory mineral dissolution in alkaline conditions will for sure play a role (Soler and Mäder, 2010), but due to the high amount of montmorillonite present in the MX-80 bentonite it is likely that at least during the initial period of interaction bentonite-OPC interfaces will behave in a similar way as Na-montmorillonite-OPC interfaces. For other interface types (e.g., Opalinus Clay-OPC or Boom Clay-OPC), a direct inference on the evolving diffusivity or porosity is difficult due to the completely different initial conditions of the interface. Nevertheless, the results of the present study may provide a general indication in terms of expected times of reactions and magnitudes of diffusivity changes.

Besides transport of solutes, as investigated in this study, many other processes are important for the assessment of the safety of a geologic repository for radioactive waste. These processes include the (re-)saturation of clay rocks or clay granulates surrounding the waste canisters, or also transport of gases (dissolved or in the gas phase). The (re-)saturation occurs via advective water transport and diffusive water vapour transport. Clay skins with reduced porosity will certainly also affect these processes, leading to a slower mass transfer in general. The performed experiments indicate an extremely low diffusivity for the anion $^{36}Cl^-$. This experimental evidence probably has consequences for other species: i) the flux of the anion OH^- through the clay at larger times is likely to be limited as well to a relative small extent; accordingly, the (initially probably fast) propagation of the pH front will later slow down. ii) In a similar way, diffusion of negatively charged radionuclides may be strongly reduced. iii) Diffusion of large dissolved gas molecules (e.g. CH_4, CO_2) will probably be influenced as well by the reactions at the interfaces, because diffusion of large gas molecules tends to occur through the same porosity as that of anions.

At the same time, a generalisation of the present findings to the much larger space and time scale relevant for a repository would certainly require additional investigations. For instance, questions of the homogeneity of heterogeneity of skins at larger spatial scales should be addressed. Also, the performed experiments on OPC paste Na-montmorillonite interfaces do not allow an extrapolation of the porosity/diffusivity behaviour over very long time scales, even though the previously discussed trends of the evolution of the diffusion coefficient suggest that in short term a total reduction of the porosity will not be reached.

5. Conclusions

Na-montmorillonite/OPC paste interface samples have been reacting under controlled condition over six years. The evolution of transport properties across the interface was periodically monitored by through-diffusion experiments. Two distinct phases of the interface reactivity could be identified. The first phase (0-17 months) was characterized by a strong decrease of the diffusion coefficient (46% reduction of D_e for HTO, and ~96% decrease of D_e for $^{36}Cl^-$). The second phase (17-73 months) was characterised by a slow further decrease of the diffusivity across the interface. Combining the diffusive flux measurements presented here and non-destructive analysis of the sample porosity across the interface presented by Shafizadeh et al. (2020), it was concluded that the changes of transport properties across the sample are dominated by a narrow low porosity / low diffusivity alteration zone in the clay compartment close to the interface. This alteration zone is likely to form as a result of precipitations following mineral transformations. A reduction of diffusive transport with time was observed for both HTO and $^{36}Cl^-$ tracers. The chloride D_e showed a much stronger reduction compared to HTO. This suggests that precipitation of new phases occurred likely in the porosity that was accessible to anions (free porosity), such that these pathways were partly blocked for $^{36}Cl^-$. The neutral tracer HTO is less affected by this partial blocking of the free porosity, because it can still diffuse via interlayer or DDL porosity. The $D_{e,\,Cl}$ values determined for the entire clay domain are very low ($<2.5 \times 10^{-13}$ m^2 s^{-1}), and in some cases no anion flux at all was observed. A complete clogging,

that is, a complete blocking of the pore space for diffusion of HTO, was, however, not observed up to a time of six years. Combining information gained from the precedent neutron investigation measurements (Shafizadeh et al., 2020) with the present data allowed estimating the diffusive properties of the skin region for HTO and chloride. These skin regions in the clay (after at least 45 months interaction) have an estimated diffusivity of 7.0 x 10^{-12} m^2 s^{-1} for HTO (considering the unaltered clay part as Na montmorillonite) and <5.1 x 10^{-14} m^2 s^{-1} for chloride. A series of assumptions and simplifications had to be made to derive these numbers, leading to comparably large uncertainties. For HTO the evolution of the effective diffusion coefficient of the entire clay domain ($D_{e,\ clay}$) and of the skin ($D_{e,\ skin}$) can be well described with Archie's empirical law, whereas for chloride the unknown accessible porosity of the skins does not allow a precise statement.

Acknowledgments

The authors would like to acknowledge Petar Bunic and Sabrina Frick for their highly appreciated support in the laboratory. Additional thanks go to Martin Glaus and Jan Tits for the many helpful discussions. Partial financial support by Nagra, the Swiss Cooperative for the Disposal of Radioactive Waste, is gratefully acknowledged.

References

Albinsson, Y., Andersson, K., Börjesson, S., Allard, B., 1996. Diffusion of radionuclides in concrete and concrete-bentonite systems. J. Contam. Hydrol. 21, 189–200.

Appelo, C.A.J., 2013. A Review of Porosity and Diffusion in Bentonite. Posiva working report 2013-29, Posiva OY, Olkiluoto, Finland

Archie, G.E., 1942. The electrical resistivity log as an aid in determining some reservoir characteristics. Trans. AIME 146, 54–62.

Beaudin, J.J., Ramachandran, V.S., Feldman, R.f., 1990. Interaction of chloride and C-S-H. Cement Concrete Res. 20, 875-883.

Berner, U., Kulik, D., Kosakowski, G., 2013. Geochemical impact of a low-pH cement liner on the near field of a repository for spent fuel and high-level radioactive waste. Phys. Chem. Earth 64, 46–56.

Bestel, M., Glaus, M.A., Frick, S., Gimmi, T., Juranyi, F., Van Loon, L.R., Diamond, L. W., 2018. Combined tracer through-diffusion HTO and ^{22}Na through Na-montmorillonite with different bulk dry densities. Appl. Geochem. 93, 158–166.

Bouchet, A., Cassagnabère, A., Parneix, J.C., 2004. Batch experiments: results on MX80. In: Michau, N. (Ed.), Ecoclay II: Effect of Cement on Clay Barrier Performance Phase II. Final report. (ANDRA) European contract FIKW-CT-2000-0028.

Boudreau, B.P., 1996. The diffusive tortuosity of fine-grained unlithified sediments. Geochim. Cosmochim. Acta 60, 3139–3142.

Bourg, I.C., Sposito, G., Bourg, A.C.M., 2006. Tracer diffusion in compacted, water-saturated bentonite. Clay Clay Miner. 54, 363–374.

Bradbury, M.H., Baeyens, 2003. Porewater chemistry in compacted re-saturated MX-80 bentonite. J. Contam. Hydrol. 61, 329-38.

Bradbury, M.H., Berner, U., Curti, E., Hummel, W., Kosakowski, G., Thoenen, T., 2014. The Long Term Geochemical Evolution of the Nearfield of the HLW Repository. Nagra Technical Report NTB 12-01, Nagra, Wettingen, Switzerland.

Carlson, L., 2004. Bentonite mineralogy. Posiva working report, 2004-02, Posiva OY, Olkiluoto, Finland.

Claret, F., Bauer, A., Schafer, T., Griffault, L., Lanson, B., 2002. Experimental Investigation of the interaction of clays with high-pH solutions: a case study from the Callovo-Oxfordian formation, Meuse- Haute Marne underground laboratory (France). Clay Clay Miner. 50, 633–646.

Crank, J., 1979. The Mathematics of Diffusion. Oxford University Press.

Cuevas, J., vigil de la Villa, R., Ramirez, S., Sanchez, L., Fernandez, R., Leguey, S., 2006. The alkaline reaction of FEBEX Bentonite: a contribution to the study of the performance of bentonite/concrete engineered barrier systems. J. Iber. Geol. 32, 151-174.

Dauzeres, A., Le Bescop, P., Sardini, P., Cau Dit Coumes, C., 2010. Physico-chemical investigation of clayey/cement-based materials interaction in the context of geological waste disposal: Experimental approach and results. Cement Concrete Res. 40, 1327–1340.

De Windt, L., Pellegrini, D., van der Lee, J., 2004. Coupled modeling of cement/claystone interactions and radionuclide migration. J. Contam. Hyrol. 68, 165-182.

Döhring, L., Görlich, S., Rüttener, W., and Schwerzmann, R., 1994. Herstellung von homogenen Zementsteinen mit hoher hydraulischer Permeabilität. Nagra Internal Report NIB 94-29, Nagra, Wettingen, Switzerland.

Fernandez, R., Rodríguez, M., Vigil de la Villa, R., Cuevas, J., 2010. Geochemical constraints on the stability of zeolites and C–S–H in the high pH reaction of bentonite. Geochim. Cosmochim. Acta, 74, 890–906.

Fernandez, R., Torres, E., Ruiz, A. I., Cuevas, J., Cruz Alonso, M., Garcia Calvo, J. L., Rodriguez, E., Turrero, J. M., 2017. Interaction processes at the concrete-bentonite interfcae after 13 years of FEBEX-Plug operation. Part II : Bentonite contact. Phys. Chem. Earth 99, 49-63.

Gaucher, E. C. and Philippe Blanc, P., 2006. Cement/clay interactions - A review: Experiments, natural analogues, and modeling. Waste Manage. 26, 776–788.

Gimmi, T., Kosakowski, G., 2011. How mobile are sorbed cations in clays and clay rocks? Environ. Sci. Technol. 45, 1443–1449.

Glaus, M.A., Baeyens, B., Bradbury, M.H., Jakob, A., Van Loon, L.R., Yaroshchuk, A., 2007. Diffusion of ^{22}Na and ^{85}Sr in montmorillonite: evidence of interlayer diffusion being the dominant pathway at high compaction. Environ. Sci. Technol. 41, 478–485.

Glaus, M.A., Rossé, R., Van Loon, L.R., Yaroshchuk, A.E., 2008. Tracer diffusion in sintered stainless steel filters: measurement of effective diffusion coefficients and implications for diffusion studies with compacted clays. Clay Clay Miner. 56, 677–685.

Glaus, M.A., Frick, S., Rossé, R., Van Loon, L.R., 2010. Comparative study of tracer diffusion of HTO, $^{22}Na^{+}$ and $^{36}Cl^{-}$ in compacted kaolinite, illite and montmorillonite. Geochim. Cosmochim. Acta 74, 1999–2010.

Glaus, M.A., Aertsens, M., Maes, N., Van Laer, L., Van Loon, L.R., 2015. Treatement of boundary condition in through-diffusion: A case study of $^{85}Sr^{2+}$ diffusion in compacted illite. J. Contam. Hydrol. 177-178, 239-248.

Glaus, M.A., Frick, S., Van Loon, L.R., 2017. Diffusion of Selected Cations and Anion in Compacted Montmorillonite and Bentonite. PSI Bericht 17-08, Paul Scherrer Institut, Villigen PSI, Switzerland.

González Sánchez, F., Van Loon, L.R., Gimmi, T., Jakob, A., Glaus, M.A., Diamond, L.W., 2008. Self-diffusion of water and its dependence on temperature and ionic strength in highly compacted montmorillonite, illite and kaolinite. Appl. Geochem. 23, 3840–3851.

Hirao, H., Yamada, K., Takahashi, H., Zibara, H., 2004. Chloride binding of cement estimated by binding isotherms of hydrates. J. Adv. Concr. Technol. 3, 77-84.

Hodgkinson, E.S., Hughes, C.R., 1999. The mineralogy and geochemistry of cement/rock reactions: high-resolution studies of experimental and analogue materials. Chem. Contain. Waste Geosphere 157, 195–211.

IAEA, 2009. Geological Disposal of Radioactive Waste: Technological Implications for Retrievability. NW-T-1.19.

Jakob, A., Sarott, F.A., Spieler, P., 1999. Diffusion and Sorption on Hardened Cement Pastes - Experiments and modelling Results. PSI Report 99-05, Paul Scherrer Institut, Villigen PSI, Switzerland

Jenni, A., Gimmi, T., Alt-Epping, P., Mäder, U., Cloet, V., 2017. Interaction of ordinary Portland cement and Opalinus Clay: Dual porosity modelling compared to experimental data. Phys. Chem. Earth 99**,** 22-37.

Mejlhede Jensen, O., Freiesleben Hansen, P., Coats, A.M., Glasser, F.P., 1999. Chloride ingress in cement paste and mortar. Cement Concrete Res. 29, 1497-1504.

Karnland, O., 2004. Laboratory experiments concerning compacted bentonite contacted to high pH solutions. In: Michau, N. (Ed.), Ecoclay II: Effect of Cement on Clay Barrier Performance Phase II. Final Report. (ANDRA) European contract FIKW-CT-2000-0028.

Karnland, O., Olsson, S., Nilsson, U., 2006. Mineralogy and sealing properties of various bentonites and smectite-rich clay materials. SKB Technical Report TR-06-30, Svensk Kärnbränslehantering AB, Stockholm, Sweden.

Kosakowski, G., & Berner, U. (2013). The evolution of clay rock/cement interfaces in a cementitious repository for low- and intermediate level radioactive waste. Phys. Chem. Earth, 64, 65–86.

Kulik, D., Wagner, T., Dmytrieva, S.V., Kosakowski, G., Hingerl, F.F., Konstantin, Chudnenko, K.V., Berner, U.R., 2013. GEM-Selektor geochemical modeling package: Revised algorithm and GEMS3K numerical kernel for coupled simulation codes. Computat. Geosci. 17, 1–24.

Mäder, U., Jenni, A., Lerouge, C., haboreau, S., Miyoshi, S., Kimura, Y., Cloet, V., Fukaya, M., Claret, F., Otake, T., Shibata, M., Lotenbach, B., 2017. 5-year chemico-physical evolution of concrete–claystone interfaces, Mont Terri Rock Laboratory (Switzerland). Swiss J. Geosci. 110, 307–327.

Martin L.H.J., Leemann, A., Milodowski, A.E., Mäder, U.K., Münch, B., Giroud, N., 2016. A natural cement analogue study to understand the long-term behaviour of cements in nuclear waste repositories: Maqarin (Jordan), Appl. Geochem. 71, 20-34.

Marty N.C.M., Munier, I., Gaucher, E.C., Tournassat, C., Gaboreau, S., Quang Vong, C., Giffaut, E., Cochepin, B., Claret, F., 2014. Simulation of Cement/Clay Interactions: Feedback on the Increasing Complexity of Modelling Strategies. Transport Porous Med. 104, 385–405.

Melkior,T., Mourzagh, D., Yahiaoui, Y., Thoby, D., Alberto, J.C., Brouard, C., N. Michau, N., 2004. Diffusion of an alkaline fluid through clayey barriers and its effect on the diffusion properties of some chemical species. Appl. Clay Sci, 26, 99– 107.

Melkior, T., Gaucher, E.C., Brouard, C., Yahiaoui S., Thoby D., Clinard C., Ferrage, E., Guyonnet D. , Tournassat, C., Coelho, D., 2009. Na^{+} and HTO diffusion in compacted bentonite: Effect of surface chemistry and related texture. J. Hydrol. 370, 9–20.

Mitchell, J.K. and Soga, K., 1992. Fundamentals of Soil Behaviour. 3rd Edition, John Wiley and Sons, 592pp.

Muurinen, A., 1994. Diffusion of anions and cations in compacted sodium bentonite. VTT Publications 168, Technical Research Centre of Finland, Espoo, Finland.

Nagra, 2002. Project Opalinus Clay – Safety Report, Demonstration of Disposal Feasibility for Spent Fuel, Vitrified High-level Waste and Long-lived Intermediate-level Waste ("Entsorgungsnachweis"). Nagra Technical Report NTB 02–05, Nagra, Wettingen, Switzerland.

Nagra, 2014. SGT-Etappe-2: Vorschlag weiter zu untersuchender geologischer Standortgebiete mit zugehörigen Standortarealen für die Oberflechenanlage: Charakteristische Dosis intervalle un unterlagen zur Bewertung der Barrierensysteme. Nagra Technical Report NTB 14-03, Nagra, Wettingen, Switzerland.

Page, C-L-. Short, N.R., El Tarras, A., 1981. Diffusion of chloride in hardened cement pastes. Cement Concrete Res. 11, 395-406.

Plusquellec, G., and Nonat, A., 2016. Interactions between calcium silicate hydrate (C-S-H) and calcium chloride, bromide and nitrate. Cement Concrete Res. 90, 89-96.

Pusch, R., 2001. The Buffer and Backfill Handbook. Part 2: Materials and Techniques. SKB Technical Report TR-02–12, SKB, Stockholm, Sweden.

Ramirez, S., Cuevas, J., Vigil, R., Leguey, S., 2002. Hydrothermal alteration of ‘‘La Serrata’’ bentonite (Almeria, Spain) by alkaline solutions. Appl. Clay Sci. 21, 257–269.

Read , D., Glasser, F. P., Ayora, C., Guardiola, M. T., Sneyers, A. (2001). Minerolgical and microstructural changes accompanying the interaction of Boom Clay with ordinary Portland cement. Adv. Cem. Res. 13, 175–183.

Rosanne, M., Mammar, N., Koudina, N., Prunet-Foch, B., Thovert, J.-F., Tevissen, E., Adler, P.M., 2003. Transport properties of compact clays. II. Diffusion. J. Colloid Interf. Sci. 260, 195–203.

Sarott, F. A., Bradbury, M.H., Pandolfo, P., Spieler, P., 1992. Diffusion and adsorption studies on hardened cement paste and the effect of carbonation on diffusion rates. Cement Concrete Res. 22, 439-444

Savage, D., 2011. A review of analogues of alkaline alteration with regard to long-term barrier performance. Min. Magazine 75**,** 2401-2418.

Savage, D., and Cloet, V., 2018. A review of Cement-Clay Modelling. Nagra Arbeitsbericht NAB 28-24, Nagra, Wettingen, Switzerland.

Shafizadeh, A., Gimmi, T., Van Loon, L.R., Kaestner, A., Lehmann, E., Mäder, U., Churakov, S.V., 2015. Quantification of water content across a cement-clay interface using high resolution neutron radiography. Phys. Proc. 69**,** 516-523.

Shafizadeh, A., Gimmi, T., Van Loon, L.R., Mäder, U., Churakov, S.V. 2019 Neutron Imaging Study of Evolution of Structural and Transport Properties of Cement-Clay Interfaces. PhD Thesis, University of Bern, Bern, Switzerland

Shafizadeh, A., Gimmi, T., Van Loon, L.R., Kaestner, A.P., Mäder, U.K., Churakov, S.V., 2020. Time-resolved porosity changes at cement-clay interfaces. Cement Concrete Res., 127, 105924.

Smellie, J.A.T., 1998. Executive Summary: Maquarin natural analogue project: Phase III. SKB Technical Report (TR 98-04), SKB, Stockholm, Sweden.

Steefel, C.I., Lichtner, P.C., 1998. Multicomponent reactive transport in discrete fractures II: Infiltration of hyperalkaline groundwater at Maquarin, Jordan, a natural analogue site. J. Hydrol. 209, 200–224.

Soler, M.J., and Mäder, U.K., 2010 Cement-rock interaction: Infiltration of a high-pH solution into a fractured granite core. Geol. Acta 8, 221-233

Taylor. H.W.F., 1997. Cement chemistry, Academic press.

Tinseau E., Bartier, D., Hassouta, L., Devol-Brown, I., Stammose, D., 2006. Mineralogical characterization of the Tournemire argillite after in situ interaction with concretes. Waste Manage. 26, 789–800.

Tits, J., Jakob, A., Wieland, E., Spieler, P., 2003. Diffusion of tritiated water and $^{22}Na^{+}$ through non-degraded hardened cement pastes. J. Contam. Hydrol. 61, 45–62.

Tyagi, M., Gimmi, T., Churakov, S.V. 2013. Multi-scale micro-structure generation strategy for up-scaling transport in clays. Adv. Water Resour. 59, 181–195.

Van Loon, L.R., Soler, J.M., 2003. Diffusion of HTO, $^{36}Cl^{-}$, $^{125}I^{-}$ and $^{22}Na^{+}$ in Opalinus Clay: effect of confining pressure, sample orientation, sample depth and temperature. Nagra Technical Report NTB 03-07, Nagra, Wettingen, Switzerland.

Van Loon, L.R., Glaus, M.A., Müller, W., 2007. Anion exclusion effects in compacted bentonites: towards a better understanding of anion diffusion. Appl. Geochem. 22, 2536–2552.

Van Loon, L.R, 2014. Effective Diffusion Coefficients and Porosity Values for Argillaceous Rocks and Bentonite: Measured and Estimated Values for the Provisional Safety Analyses for SGT-E2. Nagra Technical Report NTB 12-03, Nagra, Wettingen, Switzerland.

Van Loon, L.R. and Mibus, J., 2015. A modified version of Archie's law to estimate effective diffusion coefficients of radionuclides in argillaceous rocks and its application in safety analysis studies. Appl. Geochem. 59, 85–94.

Vieillard, P., Ramírez, S., Bouchet, A., Cassagnabère, A., Meunier, A., Jacquot, E., 2014. Alteration of the Callovo-Oxfordian clay from Meuse-Haute Marne Underground Laboratory (France) by alkaline solution: II. Modelling of mineral reactions, Appl. Geochem. 19, 1699–1709

Watson, C., Hane, K., Savage, D., Benbow, S., Cuevas, J., Fernández, R., 2009. Reaction and diffusion of cementitious water in bentonite: Results of 'blind' modeling. Appl. Clay Sci. 45, 54–69.

Wersin, P., Curti, E., Appelo, C.A.J. 2004. Modelling bentonite–water interactions at high solid/liquid ratios: swelling and diffuse double layer effects. Appl. Clay Sci. 26, 249-257

Wieland, E., Tits, J., Dobler, J.P., Spieler, P., 1998. Interaction of Eu(III) and Th(IV) with Sulphate-resisting Portland cement. Mater. Res. Soc. Symp. Proc. 506, 573–578.

Yamaguchi, T., Sawaguchi, T., Tsukada, M., Hoshino, S., Tanaka, T., 2016. Mineralogical changes and associated decrease in tritiated water diffusivity after alteration of cement–bentonite interfaces, Clay Miner. 51, 279–287.